Gaber *et al.*
Journal of Engineering and Applied Science (2022) 69:100
https://doi.org/10.1186/s44147-022-00145-w

Journal of Engineering and Applied Science

REVIEWS Open Access

Looper and tension control in hot strip finishing mills based on different control approaches

Ahmed Gaber[1*], Mahmoud Elnaggar[2] and Hossam Abdel Fattah[1]

*Correspondence: eng_ahmed_gaber@hotmail.com

[1] Electric Power Department, Faculty of Engineering, Cairo University, Giza, Egypt
[2] Electric Power and Machines Department, Faculty of Engineering, Cairo University, Giza, Egypt

Abstract

The looper control of hot strip finishing mill is one of the most critical control items in hot strip rolling mill process. It is a highly complex nonlinear system, with strong states coupling and uncertainty that present a difficult control challenge. Loopers are placed between finishing mill stands not only to control the mass flow of the two stands but also to generate a constant specific strip tension during rolling, independent of the actual strip stock which influences the width of the strip. Some of the applicable control architectures for the finishing mill are reviewed. Two general approaches are considered: the first is based on a loop or SISO (single input single output) strategy, while the second is based on a MIMO strategy:

In the loop approach, two different schemes are considered with distinct loop configuration. For both schemes, PID and fuzzy-PID are considered for comparison purposes. Since in the second scheme the most important loop is the looper control loop, it is investigated whether a nonlinear sliding mode control can significantly improve the response.

In the multi-variable or MIMO approach, standard LQR (linear quadratic regulator) is investigated after linearization of the system.

Keywords: Hot strip finishing mill, Looper control, Tension control, Fuzzy-like PID control, Sliding mode control, LQR

Introduction

A hot rolling of steel strip is a sequential process performed to convert the semi-finished slab which is reheated to a predetermined temperature and then rolled to make the specified hot strip in a coiled form. A hot slab mill primarily consists of the following units or areas (illustrated in Fig. 1): reheat furnace, roughing mill, transfer table, coil box, crop shear, finishing mill, runout table, and coiler. Slabs of around 250-mm thickness are reheated to a temperature of approximately 1200°C in the reheat furnace. In the roughing mill, the reheated slabs are reduced to a thickness of 25–50 mm. The resulting transfer bar is then transported to the finishing mill, where it is further reduced to the final thickness 0.8–20 mm.

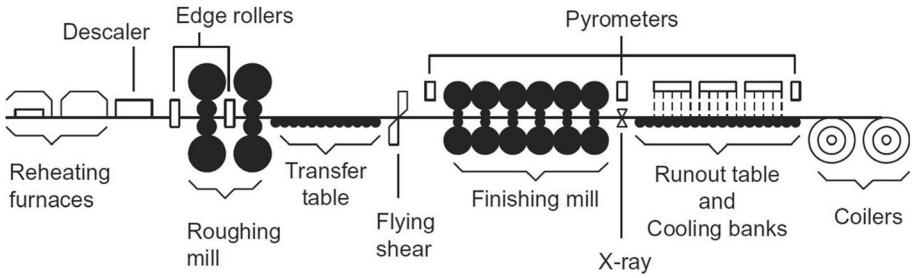

Fig. 1 The schematic diagram of a traditional hot strip mill

The finishing mill in hot strip mill has typically five to seven stands to reduce the transfer bar thickness down to the appropriate thickness. The speed of the rolling is set to perform the final reduction between 820 and 900 °C at the finishing temperature to achieve particular mechanical properties. The finishing mills roll the transfer bar in tandem, which mean each bar is rolled at once through all the finishing stands. The hot steel is quite fragile as it is rolled and tension between the stands of finishing mill must be tightly controlled at very low levels to prevent stretching or tearing the strip. The position of each roll is fed back to the finishing mill's automation system which, along with information from the load cells that monitor rolling force and from the gauge measuring final strip thickness, work to smoothly adjust the roll gaps and speeds to maintain stable rolling of strip to the necessary thickness despite the temperature variations present in every bar.

For the last three decades, many advanced looper control techniques have been proposed, such as PI controller, inverse linear quadratic ILQ [1], neuro-fuzzy methodologies [2, 3], adaptive control [4], and H_∞ [5, 6]. However, sufficient performance has not been achieved due to the following: the model is approximately linearized around the reference point; the controller ignores the interactions between the strip gauge, tension, and angle; or the external unknown nonlinear disturbances are not considered. Recently, the nonlinear sliding mode techniques have been proposed due to robustness performance and the ability to withstand external disturbance and parameter uncertainties [7, 8].

This paper's objective is to illustrate and compare the performance of different control techniques in the presence of disturbances, uncertainty, and unmodeled dynamics. The paper's goal is achieved by applying the traditional PID controller as the first control technique via two control schemes. The second controller adopted is achieved by replacing the PID controller by fuzzy-like PID in both control schemes. The super twisting sliding mode control is considered the third adopted controller technique, in which the control input is the reference of the looper torque and the controlled variable is the looper angle. The last control technique proposed in this paper is the linear quadratic regulator (LQR). All the proposed controllers have been implemented individually for a complete nonlinear six stands model.

Besides this introductory section which includes a brief introduction and the objective of this research, the paper includes four sections. The process model is introduced in the "Process model" section, the proposed controller is explained in the

"Control approaches" section, simulation results are illustrated in the "Simulation model" section, and conclusions are drawn in the "Conclusions" section.

Process model

Between all the stands of the finishing mill, a looper is installed for the purpose of ensuring that there is a particular strip tension between any two stands. The reason is to prevent the necking of the strip as a result of excessive tension. Too strong tension will finally lead to a strip break. This can occur when the mass flow through the following stand is higher than the flow through the previous stand as a result of a too high speed in the following stand. When the mass flow through the following stand is smaller, a loop is built up. A steadily increasing loop leads to the formation of folds. If a fold is formed, the strip may enter the next stand with triple strip thickness. The result may be a breakage of a roll or of a spindle. Thus, a loop control must be installed. For technological reasons, the strip tension should be kept constant between two stands, independent of the actual strip stock. Usually, the major mechanical and hydraulic components of each looper as shown in Fig. 2 are one hollow idler roll, approximately located midway between two consecutive stands: one pivoting arm which holds the roll and one rotating hydraulic actuator double.

Strip tension dynamics

The interstand strip tension $\sigma(t)$ described here is close to [7–9], which is defined by Young's modulus E of the strip and the strip stretch as the following:

$$\sigma(t) = E\left[\frac{L'(\theta) - (L + \xi(t))}{L + \xi(t)}\right] \tag{1}$$

where θ is the looper angel; L is the distance between two consecutive stands; $L^{'}(\theta)$ is the geometric strip length between stands i and $i+1$ considering the motion of the looper; and $(L+\xi(t))$ is the stored strip length, which changes as the result of mass flow difference $\xi(t)$

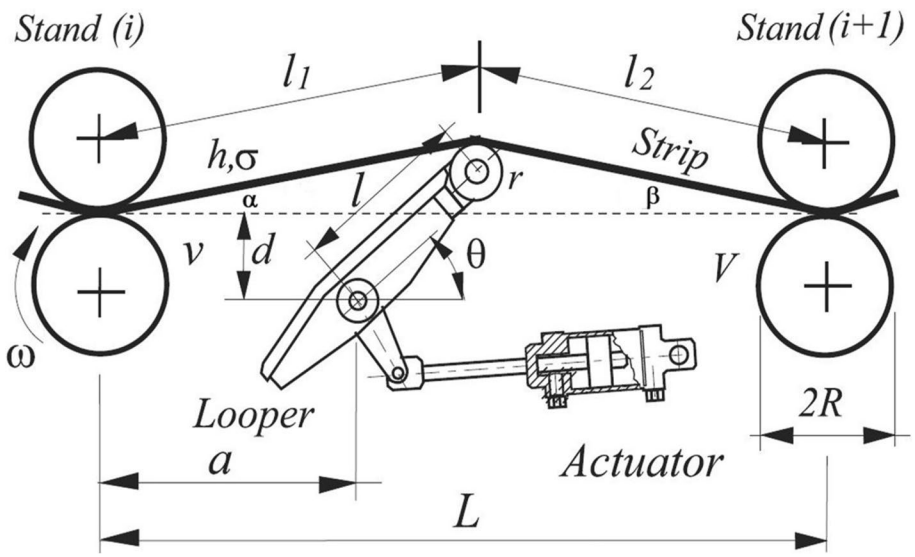

Fig. 2 Looper geometry [9]

between stands i and $i+1$. It is worth to mention that $\xi(t)$ is rather small compared with L. So $(L+\xi(t))$ is approximated to L. The equation (1) is rewritten as,

$$\sigma(t) = E\left[\frac{L'(\theta) - (L+\xi(t))}{L}\right] \tag{2}$$

The geometric length between stands $L^{'}(\theta)$ is evaluated as follows:

$$L'(\theta) = \ell_1(\theta) + \ell_2(\theta) \tag{3}$$

where $\ell_1(\theta)$, $\ell_2(\theta)$ are the strip lengths depicted in Fig. 2. It can be computed according to the following geometrical formulas:

$$\ell_1(\theta) = \sqrt{(a + l\,cos\theta)^2 + (l\,sin\theta + (r-d))^2} \tag{4}$$

$$\ell_2(\theta) = \sqrt{((L-a) - l\,cos\theta)^2 + (l\,sin\theta + (r-d))^2} \tag{5}$$

The interstand strip deviation $\dot{\xi}(t)$ with respect to the interstand length L is described by the following equation:

$$\dot{\xi}(t) = v_i(t) - V_{i+1}(t) + \omega_\xi(t) \tag{6}$$

where $v_i(t)$ is the speed of the strip leaving the stand i , $V_{i+1}(t)$ is the strip speed entering the downstream stand $(i+1)$, and $\omega_\xi(t)$ represent unmodeled dynamics.

The strip speed is controlled by automatic speed regulator. It can be modelled as first-order systems with time constant τ_v as the following:

$$\dot{v_i}(\mathrm{t}) = -\frac{1}{\tau_v} v_i(\mathrm{t}) + \frac{1}{\tau_v} v^{ref}(\mathrm{t}), \quad v_i(0) = v_0^i \tag{7}$$

The relation between the speed of the strip leaving the stand $v_i(t)$ and the angular velocity ω_i of the work rollers is evaluated as:

$$v_i(t) = \left(1 + S_f^i\right)\omega_i(t)R^i \tag{8}$$

where S_f^i represents forward slip, and R^i represents work roller radius.

The mass flow is conserved through the stand and assuming the strip width is constant, the speed $V_i(t)$ of the strip entering the ith stand can be evaluated as the following:

$$V_i(t) = \frac{v_i(t)h_i(t)}{H_i(t)} \tag{9}$$

where $H_i(t)$ and $h_i(t)$ are the stand entry thickness and the exit thickness, respectively.

Finally, the derivative of interstand tension $\sigma(t)$ is given as:

$$\dot{\sigma}(t) = \frac{E}{L}\left[\frac{d}{dt}L'(\theta) - \dot{\xi}(t)\right] \tag{10}$$

$$\frac{d}{dt}L'(\theta) = \frac{dL'}{d\theta}\frac{d\theta}{dt} \tag{11}$$

$$\frac{dL'}{d\theta} = \frac{d\ell_1}{d\theta} + \frac{d\ell_2}{d\theta} \tag{12}$$

So, $\dot{\sigma}(t)$ can be evaluated as:

$$\dot{\sigma}(t) = \frac{E}{L}\left[l[\sin(\theta+\beta) - \sin(\theta-\alpha)]\dot{\theta}(t) - \left(v_i(t) - V(t)_{i+1} + \omega_\xi(t)\right)\right] \tag{13}$$

where α and β are the angles between the strip and the pass line and given by

$$\alpha = \tan^{-1}\left[\frac{l\,sin\theta + (r-d)}{a + l\,cos\theta}\right] \tag{14}$$

$$\beta = \tan^{-1}\left[\frac{l\,sin\theta + (r-d)}{(L-a) - l\,cos\theta}\right] \tag{15}$$

Looper dynamics

Looper dynamics is obtained by applying Newton's law of motion to the looper system. Given the looper inertial momentum to hydraulic actuator J, the hydraulic actuator torque on the looper $T_u(t)$, load torque on the looper $T_{load}(\theta)$, and unmodeled dynamics $\omega_\omega(t)$, the dynamics can be expressed as:

$$J\ddot{\theta}(t) = T_u(t) - T_{load}(\theta) + \omega_\omega(t) \tag{16}$$

where $T_{load}(\theta)$ represents the loads caused by strip tension $T_\sigma(\theta)$, strip weight $T_s(\theta)$, and looper weight $T_l(\theta)$. It can be evaluated as follows:

$$T_\sigma(\theta) = \sigma hWl[\sin(\theta+\beta) - \sin(\theta-\alpha)] \tag{17}$$

$$T_s(\theta) = \rho g h^i W\left(l_1^i(\theta) + l_2^i(\theta)\right) l\,cos\theta \tag{18}$$

$$T_L(\theta) = glcos\theta\left(\frac{M_a}{2} + M_r\right) \tag{19}$$

The looper actuator torque $T_u{}^i$(t) controlled by automatic torque regulator and modelled as first-order system with time constant τ_t as the following:

$$\dot{T}_u^i(\mathrm{t}) = -\frac{1}{\tau_t}T_u{}^i(\mathrm{t}) + \frac{1}{\tau_t}T_u{}^{ref}(\mathrm{t}),\ T_u{}^i(0) = T_0^i \tag{20}$$

The stand model

There are several mathematical models available in the technical literature and choice of the most appropriate is not always easy. The Sims's model [10] is one of the most model

presented in the literature as being useful for control development. The model description follows closely that in [11]. The gap of the mill stand can be estimated by starting from evaluation of the rolling force relationship as the following:

$$F = \left(\kappa Q_p - \frac{\sigma_{in} + \sigma_{out}}{2}\right) W\sqrt{R'\delta} \tag{21}$$

where F is the roll force, κ is the constrained yield stress of the material, Q_p is a geometrical factor which represents the contribution of the friction and inhomogeneities of deformation [11], $(\sigma_{in}+\sigma_{out})/2$ is the mean tension stress of the strip, and $\sqrt{R'\delta}$ is the contact arc between the strip and work rolls given in terms of the radius of the flattened roll $R^{'}$ and the reduction of $\delta = (H_i - h_i)$.

The deformed work roll radius $R^{'}$ is obtained using the Hitchcock equation as the following [12]:

$$R' = R\left(1 + \frac{16\left(1-\upsilon^2\right)P}{\pi E \Delta h}\right. \tag{22}$$

where R represents the undeformed work roll radius, υ is Poisson's ratio, and E is Young's modulus.

The geometrical factor Q_p as expressed in Sims's paper is a non-linear function of the work roll radius (R), entry thickness H_i and exit thickness h_i:

$$Q_p = \frac{\pi}{2} a \tan^{-1}\sqrt{\frac{r}{1-r}} - \frac{\pi}{4} - ab \ln\left(\frac{Y}{h_i}\right) + \frac{1}{2} ab \ln\left(\frac{1}{1-r}\right) \tag{23}$$

$$a = \sqrt{\frac{1-r}{r}} \tag{24}$$

$$b = \sqrt{\frac{R'}{h_i}} \tag{25}$$

and the reduction r is given by:

$$r = \frac{H_i - h_i}{H_i} \tag{26}$$

$$Y = h_i + R'\phi_n^2 \tag{27}$$

where Y is an approximation evaluation of the strip thickness at the neutral plane (shown in Fig. 3) and ϕ_n presents the angle between the centre line of the stand and the neutral plane.

The angle ϕ_n is approximated as:

$$\phi_n \cong \frac{1}{b}\left(\tan\left(\frac{\pi}{8}\frac{\ln(1-r)}{b} + \frac{1}{2}\tan^{-1}\sqrt{\frac{r}{1-r}}\right)\right) \tag{28}$$

The strip thickness h_i at the mill exit is evaluated using the linearized relation as:

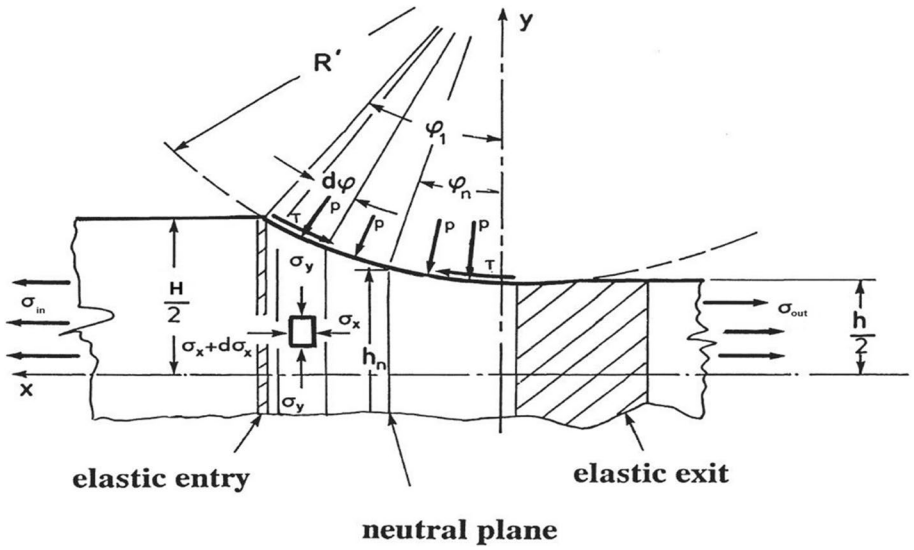

Fig. 3 Roll bite area [13]

$$h_i = S_i + \frac{F_i}{M_i} \tag{29}$$

where S_i is the position of the roll bite position actuator, F_i is the total rolling force (equal to P times W, where W is the strip width), and M_i is the mill modulus, which represents the amount of deformation of the mill stand under rolling force F_i.

The forward slip S_f^i is a measure of the relative difference between the speed of the strip exiting the roll bite and the peripheral speed of the roll. It is defined as:

$$S_f^i = \frac{V_i(t) - v_i(t)}{V_i(t)} \tag{30}$$

where v_i is the exit strip speed and V_i is entry strip speed [13]. In this model, the forward slip is expressed as [11]:

$$S_f^i = \frac{R'}{h_i}(\beta_n)^2 \tag{31}$$

$$\beta_n = \frac{\phi_1}{2} - \frac{\delta\kappa + \sigma_{in}H_i + \sigma_{out}h_i}{4\kappa R_p \mu} \tag{32}$$

$$\phi_1 = \sqrt{\frac{\delta}{R_p}} \tag{33}$$

According to [14], the friction coefficient μ presented as empirical formula obtained for flat hot rolling mill in terms of workpiece temperature on degrees F and given as:

$$\mu = 2.7x10^{-4}\ T_F - 0.08 \tag{34}$$

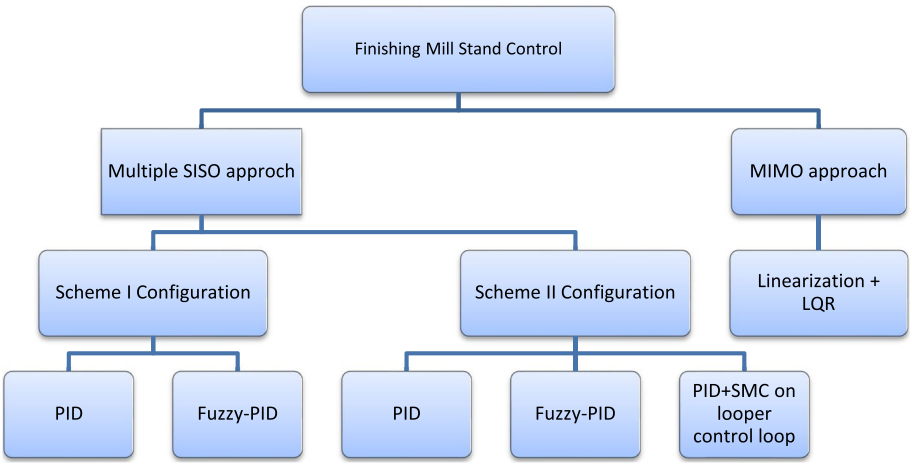

Fig. 4 Control architectures for finishing mill

The hydraulic cylinder controlled by AGR are modelled as first-order system with time constant τ_s as the following:

$$\dot{S}^i(\mathrm{t}) = -\frac{1}{\tau_s}S^i(\mathrm{t}) + \frac{1}{\tau_s}S^{ref}(\mathrm{t}), S^i(0) = S_0^i \tag{35}$$

While the exit gauge h^i which depends on the mill modulus M, roll force F^i, and roll gap S^i [15] is given as:

$$\Delta h^i(t) = \Delta S^i(t) + \frac{\Delta \mathrm{F}^i(t)}{M^i} \tag{36}$$

The deviation of the rolling force from desired point is approximated by the following linear expression.

$$\Delta F_i(t) = \left(\frac{\partial F_i}{\partial H_i}\right)\Delta H_i + \left(\frac{\partial F_i}{\partial h_i}\right)\Delta \mathrm{h}_i + \left(\frac{\partial F_i}{\partial \sigma_{i-1}}\right)\Delta\sigma_{i-1} + \left(\frac{\partial F_i}{\partial \sigma_i}\right)\Delta\sigma_i + \Delta F_{di} \tag{37}$$

where H^i is the thickness of the strip entering the stand, σ_b^i is the strip back tension, σ_f^i is the strip front tension, and $F_{di}$is the disturbance of rolling force [16].

Control approaches

Many methods have been proposed and discussed for looper tension control. In this section, some of the applicable control architectures for the finishing mill are reviewed as shown in Fig. 4. The most common traditional PID schemes represented in the "PID controller" section. In the "Fuzzy controller" section, the control system based on fuzzy-PID controller is proposed to replace the convention PID regulation in the "PID controller" section.

Nonlinear sliding mode control will be introduced in the "SMC technique" section and it is shown that in order to solve the sliding mode common problem (referred to as "chattering phenomenon"), the super twisting algorithm in implementations of sliding mode control techniques has been suggested. In the "Linear quadratic regulator"

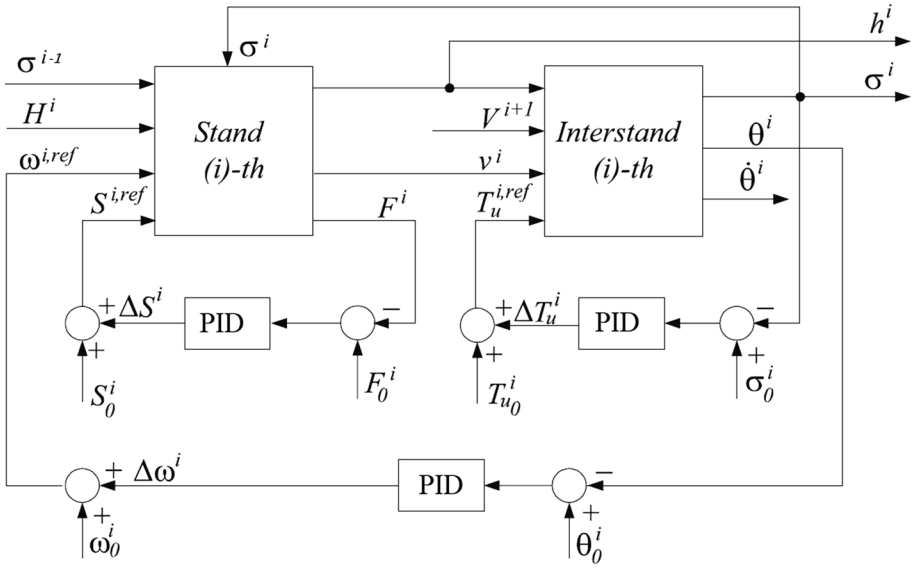

Fig. 5 Conventional PID control scheme (I) [9]

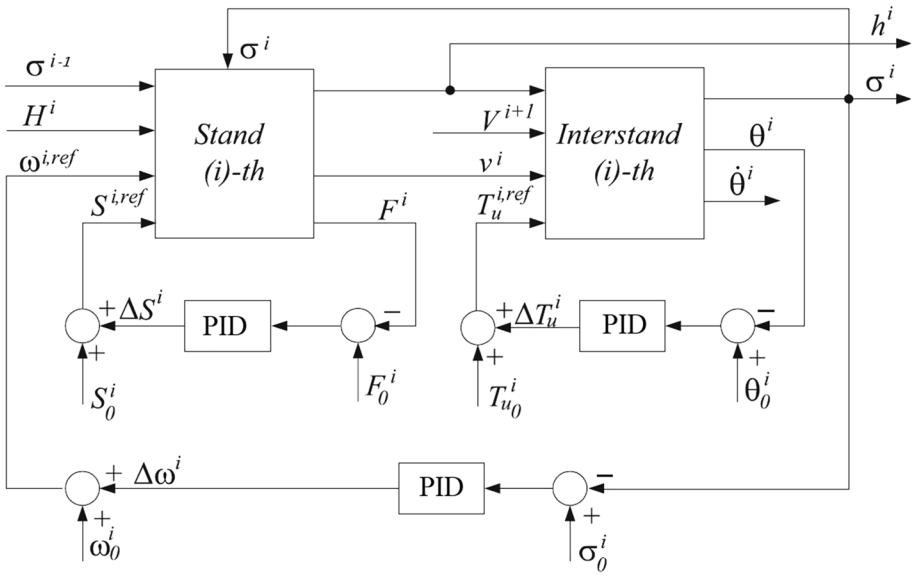

Fig. 6 Conventional PID control scheme (II) [9]

section, multivariable controller is decentralized with respect to the stands which will result in a separate LQR design for each stand/interstand zone.

PID controller

Two control loop configurations are studied in this work. The configurations are illustrated in Figs. 5 and 6. In the first control scheme, the conventional solution for regulation of thickness, angle, and tension is shown in Fig. 5. In this scheme: the looper angle deviation $\Delta\theta^i(t) = \theta_0^i - \theta^i(t)$ is regulated by ASR based on a PID controller acting on the speed reference $\omega^{i,\,ref}(t)$, the tension deviation $\Delta\sigma^i(t) = \sigma_0^i - \sigma^i(t)$ is regulated by

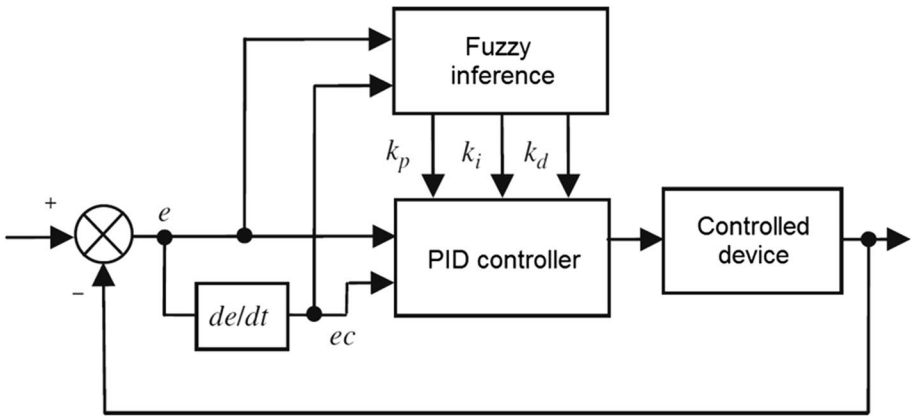

Fig. 7 Structure of fuzzy-like PID controller

ATR based on PID controller that acts on the reference torque of the looper $T_u^{i,ref}(t)$, and the force deviations $\Delta F^i(t) = F_0^i - F^i(t)$ is regulated by AGR based on PID regulator action on roll gap reference $S^{i,\,ref}(t)$ of the capsule [9, 17, 18].

In the second control scheme (Fig. 6), the solution for regulation of angle, tension, and thickness proposed works oppositely to first control schemes. The ASR based on PID controller is used to regulate the tension deviations $\Delta\sigma^i(t) = \sigma_0^i - \sigma^i(t)$ by trimming reference speed $\omega^{i,\,ref}(t)$ of upstream stand, whereas the ATR based on PID controller is used to regulate looper angle deviation $\Delta\theta^i(t) = \theta_0^i - \theta^i(t)$ by trimming the reference torque $T_u^{i,ref}(t)$ of the looper arm. The AGC uses PID controller to regulate the force deviations $\Delta F^i(t) = F_0^i - F^i(t)$ by changing the capsule position $S^{i,\,ref}(t)$.

Fuzzy controller

The PID controller techniques are widely used in practice, due to the simplicity in tuning and implementation. However, the convention schemes have a problem that high gain causes overshoot and instability whereas low gain gives a low response. So fuzzy-PID controller is proposed which gives dynamic gain based on the error and the rate of error change.

The two-dimensional fuzzy controller as shown in Fig. 7 is the most commonly used controller form in fuzzy control. The controller has a structure that is quite similar to the PID. The fuzzy inference provides the tuning to PID parameters K_p, K_i, and K_d using a nonlinear mapping from the error and its derivative

The fuzzification process

Fuzzification is the process which transforms numerical form input variables into linguistic variables. In other words, it is mapping inputs to the FLC into fuzzy set membership. In this paper, the domain of language variable of input, system error *e*, and the rate of error *ec* are {−1, −0.6665, −0.3332, 0, 0.3332, 0.6665, 1}, and the fuzzy sets are {NB, NM, NS, Z, PS, PM, PB}. The elements of the subset stand for the following: negative big, negative medium, negative small, zero, positive small, positive medium, positive big. Figure 8 shows the fuzzy membership function for *e* and *ec*, where the number of membership functions and type of membership function are chosen to be such as triangular.

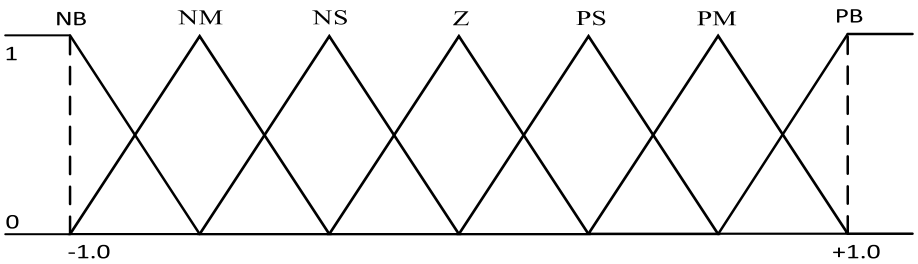

Fig. 8 The membership function of *e*, *ec*

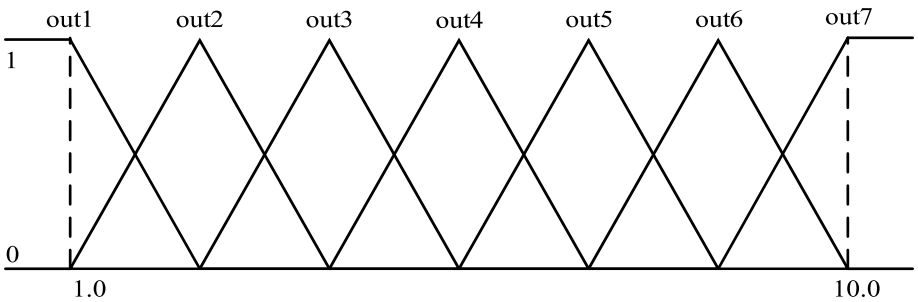

Fig. 9 The membership function of the outputs

The domain of the language variable of the output,ΔK_p,ΔK_i,ΔK_d are {1, 2.503, 3.952, 5.5, 7.03, 8.47, 10}, and the fuzzy sets are {out1, out2, out3, out4, out5, out6, out7}. The elements of the subset stand for output1: output7. Figure 9 shows the fuzzy membership function forΔK_p,ΔK_i,ΔK_d, where the number of membership functions and type of membership function is chosen to be such as triangular.

The fuzzy rule base consists of a set of consequent linguistic rules of the form if-then statements (e.g. Table S1).

The K_p coefficient is to improve the regulation accuracy and speed up the time response of the system, but if K_p is relatively high, it results in overshoot and consequently system instability; the K_i coefficient is to eliminate the steady-state error of the system, but if K_i is relatively high, it leads to integrator wind-up and leads to overshoot; the K_d coefficient is to increase the stability of the system, reduce the overshoot, and improve the transient response, but if K_d is relatively high, it produces a highly oscillatory response due to noise amplification. Based on the above discussion, the relationship between deviation *e*, the rate of deviation *ec*, and the parameters K_p, K_i , K_d could be summarized as the following:

When the absolute value of the error is large, K_p should be large and K_d should be small to achieve a better fast-track performance and the integration action should be limited to avoid a big overshoot.

When the absolute value of the error is in the middle-size, K_p should be smaller and K_i should be appropriate to avoid the system overshoot; in this case, the value of K_d term will generate a great impact on the system response.

When the absolute value of the error is small, K_p and K_i should be big to achieve a good steady-state performance, the value of K_d should be appropriate to avoid system settings near the oscillation, and the value of K_d should be appropriate. Table S1 translates the general discussion above to a set of implementable fuzzy control rules.

Defuzzification

The centre of area method is used to convert the fuzzy set to a crisp output value and the controller is obtained.

$$\Delta K_p = f_1(e, ec) = \frac{\sum_{i=1}^{n} \mu_i(e, ec) K_{Pi}}{\sum_{i=1}^{n} \mu_i(e, ec)} \tag{38}$$

$$\Delta K_i = f_2(e, ec) = \frac{\sum_{i=1}^{n} \mu_i(e, ec) K_{Ii}}{\sum_{i=1}^{n} \mu_i(e, ec)} \tag{39}$$

$$\Delta K_d = f_3(e, ec) = \frac{\sum_{i=1}^{n} \mu_i(e, ec) K_{Di}}{\sum_{i=1}^{n} \mu_i(e, ec)} \tag{40}$$

where ΔK_p, $\Delta K_i and \Delta K_d$ are scaling factors (fuzzy tuning output); K_{Pi}, K_{Ii}, and K_{Di} represent the outputs variables; μ is the membership function of fuzzy set; and n represents the number of the single-point set.

According to the fuzzy control model of each parameter and the membership assignment table of each fuzzy subset, the fuzzy matrix can be obtained for PID parameters as the following:

$$K_p = \Delta K_p * K_p' \tag{41}$$

$$K_i = \Delta K_i * K_i' \tag{42}$$

$$K_d = \Delta K_d * K_d' \tag{43}$$

where K_p, K_i, and K_d are online calculated PID gains and K_p', K_i', and K_d' are the PID parameters of conventional PID.

Fuzzy-PID for looper tension control

According to the above-mentioned design method and the control architecture illustrated in Fig. 10, the fuzzy-PID controller is applied to the first scheme in the "Fuzzy-PID control using the first scheme (I)" section and the second scheme in the "Fuzzy-PID control using the second scheme (II)" section.

Fuzzy-PID control using the first scheme (I)

The tension error (44) and its derivative (45) are controlled by a fuzzy-PID controller that acting on the reference torque of the looper $T_u^{i,ref}(t)$ (see Fig. 11).

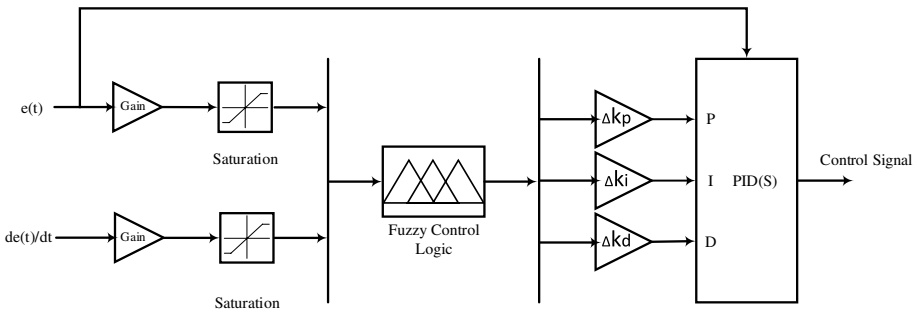

Fig. 10 The simulation block diagram of the fuzzy-PID controller

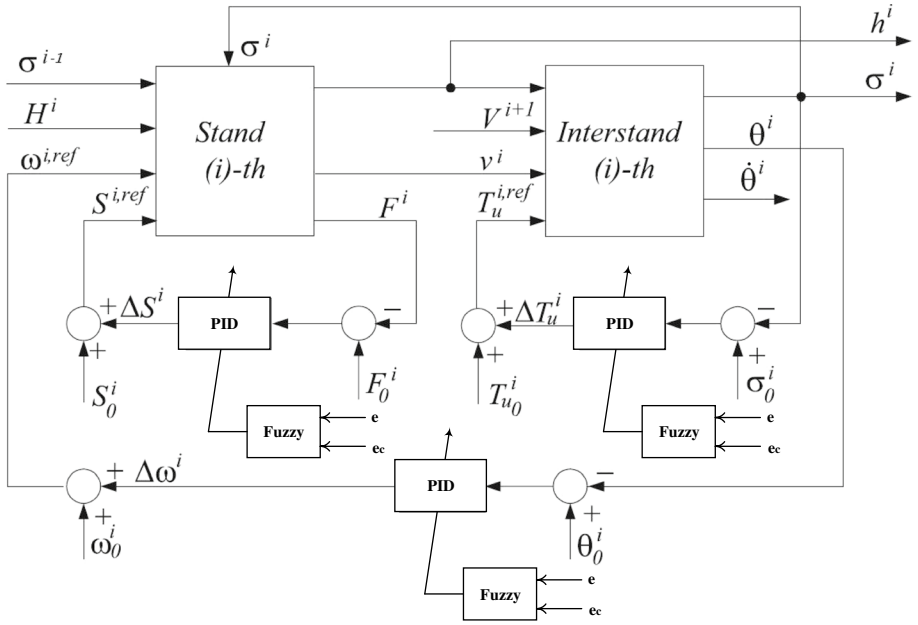

Fig. 11 Fuzzy-PID control scheme (I)

$$\Delta\sigma^i(t) = \sigma_0^i - \sigma^i(t) \tag{44}$$

$$\dot{\sigma}(t) = \frac{E}{L}\left[\frac{d}{dt}L'(\theta) - \dot{\xi}(t)\right] \tag{45}$$

The looper angle deviation (46) and its derivative (47) are controlled by a fuzzy-PID acting on the speed reference $\omega^{i,\,ref}(t)$.

$$\Delta\theta^i(t) = \theta_0^i - \theta^i(t) \tag{46}$$

$$\dot{\theta}(t\,) = \int \frac{1}{\mathrm{J}}[T_u(t) - T_{load}(t)] \tag{47}$$

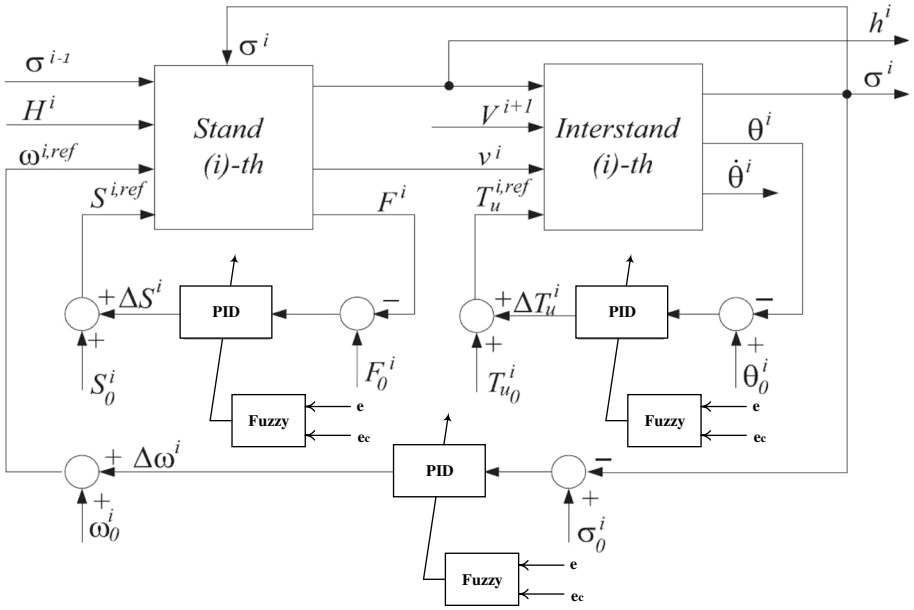

Fig. 12 Fuzzy-PID control scheme (II)

Thus, force error (48) and its derivative (37) are controlled by a fuzzy-PID controller that operates on the roll gap reference $S^{i,\,ref}(t)$.

According to the above-mentioned design method and to control architecture illustrated in Fig. 7, the tension error and the derivative of tension (13) are controlled by a fuzzy-PID controller that acts on the reference torque of the looper $T_u^{i,ref}(t)$. The looper angle deviation and the angle derivative (48) are controlled by a fuzzy-like PID acting on the speed reference $\omega^{i,\,ref}(t)$ relative to the *i*th stand, the force error and the force error rate of change controlled by a fuzzy-like PID controller that operates on the roll gap reference $S^{i,\,ref}(t)$ of the hydraulic capsule

$$\Delta F^i(t) = F_0^i - F^i(t) \tag{48}$$

Fuzzy-PID control using the second scheme (II)

In this scheme, the tension error (44) and its derivative (45) are controlled by a fuzzy-PID controller that acts on the reference speed of the looper $\omega^{i,\,ref}(t)$. The looper angle deviation (46) and its derivative (47) are controlled by a fuzzy-PID acting on the torque reference $T_u^{i,ref}(t)$. The force error (48) and its derivative (37) are controlled by a fuzzy-PID controller that operates on the roll gap reference $S^{i,\,ref}(t)$ of the hydraulic capsule relative to the *i*th stand where the force reference is decided according to the exit target thickness (see Fig. 12).

SMC technique

The inaccuracy between the mathematical model and the actual plant during formulation of any control problem arises from simplified representation of the system's dynamics and/or unknown plant parameters [19]. The robust control methods which are

supposed to achieve the desired performance in the presence of disturbance/unmodeled dynamics are the so-called sliding mode control technique.

Let us consider the single-input dynamic system

$$x^{(n)} = f(\mathbf{x}) + b(\mathbf{x})u \tag{49}$$

where the scalar $\mathbf{x}$ is the output of interest, the scalar u is the control input, and $\mathrm{x} = \left[x, \dot{x}, \ldots, x^{(n-1)}\right]^T$ is the state vector. The function $f(\mathbf{x})$ is, in general, nonlinear and not precisely known but its norm is assumed to be upper bounded by a known continuous function of $\mathbf{x}$; similarly, the control gain $b(\mathbf{x})$ is, in general, nonlinear and partially or fully unknown but is of known sign and is bounded by known, continuous function of the $\mathbf{x}$.

The control problem is to get the state x to track desired time-varying state trajectory $\mathbf{x}_d = \left[x_d\, \dot{x}_d \ldots x_d^{(n-1)}\right]^T$ in the presence of modelling uncertainties in $f(\mathbf{x})$ and $b(\mathbf{x})$.

Let us consider $\widetilde{\mathbf{x}} = \mathbf{x} - \mathbf{x}_d$ be the tracking error in the variable $\mathbf{x}$, and let $\widetilde{\mathbf{x}} = \mathbf{x} - \mathbf{x}_d = \left[\widetilde{x}\ \ \widetilde{\dot{x}} \ldots \tilde{x}^{(n-1)}\right]^T$ be the tracking error vector. Now, the sliding surface $S(t)$ can be defined as a time-varying surface in state space $R^{(n)}$ by the scalar equation $s(\mathbf{x}; t) = 0$ and λ is a strictly positive constant.

$$s(\mathbf{x};\, t) = \left(\frac{d}{dt} + \lambda\right)^{n-1} \widetilde{x} \tag{50}$$

Given the initial condition $\mathrm{x}_d(0) = \mathrm{x}(0)$, the tracking problem $\mathrm{x} = \mathrm{x}_d$ is similar to remaining on the sliding surface $s(t)$ for all $t > 0$; indeed, $s = 0$ represents a linear differential equation whose unique solution is $\widetilde{x} = 0$. Thus, keeping the scalar s quantity at zero will simplify the tracking problem of n-dimensional vector x_d to be first-order problem.

Keeping the scalar $s = 0$ can be achieved by suitably choosing the control law u in (49) such that

$$\frac{1}{2}\frac{d}{dt}s^2 \le -\varepsilon|s| \tag{51}$$

where ε is a strictly positive constant. Condition (51) (called sliding condition) makes $s(t)$ an invariant set. It is worth to mention that condition (51) forces the state trajectories to the surface $s(t)$ and, once on the surface, the system trajectories remain on the surface itself.

The block diagram of our control scheme is shown in Fig. 13. The angle deviation $\Delta\theta^i(t) = \theta_0^i - \theta^i(t)$ is controlled by trimming the reference torque $T_u^{i,ref}(t)$, tension deviations $\Delta\sigma^i(t) = \sigma_0^i - \sigma^i(t)$ by a PID controller acting on the reference $\omega^{i,\,ref}(t)$ of the upstream stand, and the AGC uses a PID controller to regulate the force deviations $\Delta F^i(t) = F_0^i - F^i(t)$ by changing the capsule position $S^{i,\,ref}(t)$

The SMC is applied to the looper angle loop as shown in Fig. 13. The procedure described here is similar to [8]. In order to apply the SMC, the equation of the looper angle need to be written in standard form as follows

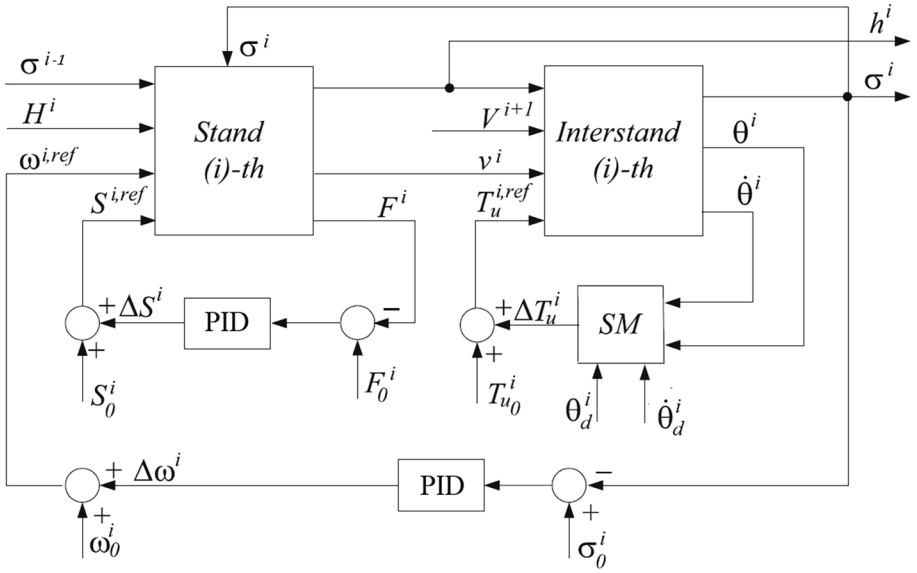

Fig. 13 SMC control structure

$$f(x) = -\frac{1}{J}\left(T^i_{load}\left(\theta^i, t\right)\right) \tag{52}$$

$$b(x) = \frac{1}{J} \tag{53}$$

where $x = \left[\theta^i(t), \dot{\theta}^i(t)\right]^T$. In order to apply SMC, the $T^i_{load}\left(\theta^i, t\right)$ is needed to be approximated. The measured value of the hydraulic torque $\hat{T}^i_u(t)$ represents an approximation of $f(x)$ since the angular acceleration of the looper is small.

The looper load torque $T^i_{load}(\theta)$ can be approximated by the measure of the hydraulic torque $\hat{T}^i_u(t)$ and looper actuator torque can be approximated by $T^{i,ref}_u(t)$. The upper bounds of the approximation errors are as follows:

$$\left|T^i_{load}(\theta) - \hat{T}^i_u(t)\right| \leq f_1 \tag{54}$$

$$\left|T^{i,ref}_u(t) - T^i_u(t)\right| \leq f_2 \tag{55}$$

The sliding surface is given by $S(t) = \overset{\sim}{\dot{\theta}}^i(t) - \lambda\overset{\sim}{\theta}^i(t)$, where

$$\overset{\sim}{\theta}^i(t) = \theta^i(t) - \theta^i_d(t) \tag{56}$$

$$\overset{\sim}{\dot{\theta}}^i(t) = \dot{\theta}^i(t) - \dot{\theta}^i_d(t), \tag{57}$$

where $\dot{\theta}_d^i(t)$is the target angular speed and $\alpha_d^i(t)$is the angular acceleration of the looper. According to the standard SMC procedure [19], the control law can be obtained as the following

$$T_u^{i,ref}(t) = \left(\hat{T}_u^i(t) + J\left(\alpha_d^i(t) - \lambda\tilde{\ddot{\theta}}^i(t)\right) - K\ \text{sign}\left[S^i(t)\right]\right. \tag{58}$$

By choosing $K \geq f_1 + f_2 + \varepsilon J$, we can now guarantee that (51) is verified. In order to eliminate the well-known chattering, Sims [10] suggests replacing the following discontinuous

$$u = -K\ \text{sign}\left[S^i(t)\right] \tag{59}$$

With

$$u = -K\left(\frac{S^i(t)}{\varnothing}\right)^2 signS^i(t) \qquad \text{if } \left|S^i(t)\right| < \varnothing \tag{60}$$

Also, Hongwei et al. [7] suggest a high slope saturation function instead of the signum function as a solution for chattering phenomena. The control low can be expressed by

$$T_u^{i,ref}(t) = \left(\hat{T}_u^i(t) + J\left(\alpha_d^i(t) - \lambda\tilde{\ddot{\theta}}^i(t) - K\ sat\left[S^i(t)/\epsilon\right]\right.\right. \tag{61}$$

where the saturation function $sat(\cdot)$ is defined by

$$sat(x) = \begin{cases} x, & |x| \leq 1 \\ \text{sign}(x), & |x| > 1 \end{cases}$$

In this paper, we suggest to use a second-order SMC algorithm the so-called super twisting sliding mode control.

Second-order sliding mode control algorithms are a powerful alternative that completely solves the chattering issue without compromising the robustness properties as well. Since the control law is a continuous function of time as it is shown in Fig. 14 and can be written as

$$u = -\text{K}\sqrt{|s|}\ \text{sgn}(s) + w \tag{62}$$

$$\dot{w} = -W\ \text{sgn}(s) \tag{63}$$

where W is a positive constant. The control low (61) can be written as

$$T_u^{i,ref}(t) = \left(\hat{T}_u^i(t) + J\left(\alpha_d^i(t) - \lambda\tilde{\ddot{\theta}}^i(t)\right) - \text{K}\sqrt{|s|}\ \text{sgn}(s) + w\right. \tag{64}$$

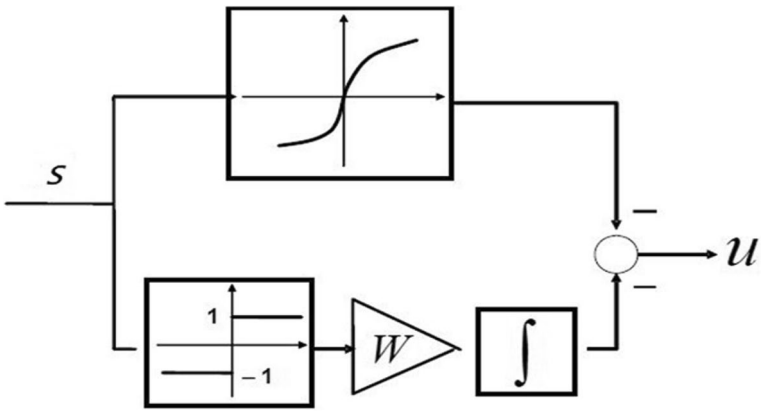

Fig. 14 Super twisting algorithm

Linear quadratic regulator

The proposed multivariable controller is decentralized with respect to the stands which will result in a separate LQR design for each stand/interstand zone.

The objective is to regulate stand speed, looper torque, and roll gap for each stand/interstand to guarantee system stability in the presence of the disturbances affecting that zone. We consider a system described by the following state equation:

$$\dot{x} = Ax + Bu, \quad t \geq 0 \qquad x(0) = x_0 \tag{65}$$

$$y = \mathrm{Cx} \tag{66}$$

where $\mathrm{A} \in R^{nxn}$, $\mathrm{B} \in R^{nxm}$, $\mathrm{C} \in R^{pxn}$ are state matrix, input matrix, and output matrix, respectively.

$x \in R^n$ is a vector, whose elements represent the individual state variables, and $u \in R^m$ is a vector whose elements represent the individual control variables. $y \in R^m$ is a vector whose elements represent the individual output variables.

The optimal control problem is defined in terms of minimizing the performance index:

$$J = \frac{1}{2}\int_0^T \left(x^T Qx + u^T Ru\right)dt \tag{67}$$

where $Q = Q^T$ is positive (semi-) definite matrix. The problem solution is obtained by solving Riccati equation:

$$A^T P + PA - \mathrm{P}BR^{-1}B^T P + Q = 0 \tag{68}$$

where $P \in R^n$ is the solution of algebraic Riccati Equation which results in the control law.

$$u(t) = Kx(t) \tag{69}$$

The feedback gain K is called the LQR (linear quadratic regulator) gain or optimal regulator gain and can be written as

Table 1 Stand#*i* state, control, and output vectors

State vector	Control vector	Output vector
$x_{i1}(\sigma_i)$	$U_{i1}(S_i)$	$y_{i1}(h_i)$
$x_{i2}(S_i)$	$U_{i2}(\omega_i)$	$y_{i2}(\sigma_i)$
$x_{i3}(T_{ui})$	$U_{i3}(T_{ui})$	$y_{i3}(F_i)$
$x_{i4}(\omega_i)$		$y_{i4}(\theta_i)$
$x_{i5}(\theta_i)$		
$x_{i6}(\dot{\theta}_i)$		
$x_{i7}(F_{ui})$		

Table 2 Stand#6 state, control, and output vectors

State vector	Control vector	Output vector
$x_{62}(S_i)$	$U_{61}(S_i)$	$y_{61}(h_i)$
$x_{67}(F_{ui})$		$y_{63}(F_i)$

$$K = -R^{-1}B^T P \tag{70}$$

For the controller design, the nonlinear model was linearized about the operating values and for the simplicity $Q(x)=I$, $R(x)=\rho I$,where, $\rho>0$. The variables represented by the elements of the state, control, and output vectors are shown in Table 1 for Stand#1:5 and Table 2 for Stand#6.

Simulation model

The dynamic simulations using MATLAB/Simulink were carried out to evaluate and compare the controllers' performance. Each controller is simulated individually to illustrate its performance. The simulation runs for 20 s where the disturbance (71) presented after 2 s from simulation running time. Here, for the sake of completeness, the parameters were obtained from a real plant for the purpose of making the simulation models behave as exactly as possible.

The values of the parameters used in the dynamic model of the looper and tension system are reported in the "Operation values" section. The comparisons, based on the mean value, standard deviation, and the error in each stand, are presented in the "PID controller parameters" section.

Looper characteristics

The simulation result based on the looper mechanism depicts in Fig. 2 with geometry data listed in Table 3.

Operation values

The dynamic simulations using MATLAB/Simulink are performed with the operation values shown in Table 4.

Table 3 The looper geometry main data

Variable	Symbol	Value	Unit
Looper roll diameter	r	240	mm
Looper arm length	l	547	mm
Distance between mill stands	L	5900	mm
Distance between the pivot point and upstream stand	a	2420	mm
Pivot point distance from the pass line	d	221	mm
Looper inertial momentum to the hydraulic actuator	J	250	Kgm^2
Operating position	θ	25 °	degree
Looper roller weight	M	500	kg

Table 4 Operation values

	Force	Specific tension [N/mm^2]	Backward tension [kN]	Roll gap [mm]
ST#1	2.3554e+07			0.014088
ST#2	2.2180e+07	4.05	79.29	0.007467
ST#3	1.8392e+07	9.25	105	0.004467
ST#4	1.6363e+07	12.6	92.33	0.003718
ST#5	9.868e+06	12.2	75.5	0.003675
ST#6	9.691e+06	12.9	70.7	0.00287
	Speed [rad/sec]	Work roll radius [mm]	Looper torque T_u [kN.m]	$\tau_v/\tau_s/\tau_l$ [sec]
ST#1	4.14	398.26	7.29	0.1592/0.032/0.0232
ST#2	6.85	397.24	5.41	0.1592/0.032/0.0232
ST#3	10.67	401.19	4.47	0.1592/0.032/0.0232
ST#4	14.28	378.96	4.197	0.1592/0.032/0.0232
ST#5	21.34	289.91	4.033	0.1592/0.032/0.0232
ST#6	25.7	294.57		0.1592/0.032/0.0232

PID controller parameters

One of the tested controllers is PID controller. The PID controller's parameters, listed in Tables S2 and Table S3, are obtained using automatic PID tuner in MATLAB/Simulink software for scheme I and scheme II respectively.

Simulation scenario

After 2 s from simulation running time, the unmodeled dynamics [8] mentioned in (13) presented as a summation of two sin functions with phase shift multiplied by the percentage of the stand entry speed as the following,

$$\omega_{\xi}(t) = 0.05\ V^i + 0.01(\sin(12t + 8) + \sin(6t)) \tag{71}$$

In both control schemes proposed, the simulation is carried out for 20 s with disturbance presence after 2 s from the running time. The mean value, summation of error square of the states, and standard deviation are calculated for comparison purposes. The data are shown in Table S4, Table S5, and Table S6 respectively. The simulation results of the stand exit thickness, roll gap, the tension between stands, looper angle,

and looper torque are shown in Figures S1, S2, S3, S4, S5, S6, S7, S8, S9, S10, S11, S12, S13, S14, S15, S16, S17, S18.

In light of the figures, one can notice that the first control scheme's response to the disturbance presented at $t \geq 2$ s from simulation running time is better than the second control scheme in terms of strip thickness and gap position overshoot. Moreover, in both control schemes, the overshoot decreased by replacing traditional PID by fuzzy-like PID. The SMC had by far the lowest overshoot percentage followed by LQR.

The first control scheme's results show the strip exit thickness and gap position tend to be close to the mean value compared to the results from the second control scheme, while the second control scheme's results of looper position and looper torque are close to the mean value compared to the first control scheme. The standard deviation values become closer to the mean value when traditional PID is replaced by Fuzzy-PID. The standard deviation values show that the overall SMC results are better than LQR results. It is also noticeable the significant difference between the error summation results of SMC and LQR on the one hand and traditional control and Fuzzy on the other hand. However, The SMC has presented better results than LQR.

Conclusions

In this paper, two control schemes have been studied with different control techniques. It was shown that the Automatic Gage Regulator compensates the disturbances much better than the second control scheme, while the second control scheme compensates the disturbances in looper position better than first control scheme. Although, in both control schemes, the performance improved when PID was replaced by fuzzy-like PID.

A multivariable controller is proposed; the benefit of using LQR controller reduces the interaction and provides stability in the presence of disturbance and unmodeled dynamics better than traditional PID even after being replaced by fuzzy-like PID. However, the effectiveness of looper and tension control approach based on the super twisting sliding mode algorithm, thanks to its robustness and structure simplicity, makes the interaction between the looper angle and tension less serious than usual and achieved much better compensation for the disturbances.

Abbreviations

$T_u(t)$	Actuator torque on the looper
φ_n	Angle at neutral plane
AGR	Automatic gap regulator
ASR	Automatic speed regulator
ATR	Automatic torque regulator
κ	Constrained yield stress
B	Control matrix
$u(t)$	Control signal
$R(x)$	Control weighting matrix
R'	Deformed work roll radius
K_d	Derivative gain
$\xi(t)$	Deviation of interstand strip length with respect to L
$\ell_1(\theta)$	Distance between stand i and looper pivot
$\ell_2(\theta)$	Distance between looper pivot and stand $i+1$
a	Distance between the pivot point and upstream stand
β	Downstream strip angle
$e(t)$	Error
S_f^i	Forward slip

μ	Friction coefficient
$L'(\theta)$	Geometric looper length between stands
Q_p	Geometrical factor
g	Gravitational constant
K_i	Integral gain
L	Interstand length
ILQ	Inverse linear quadratic
LQR	Linear quadratic regulator
$T_{load}(\theta)$	Load torque on the looper
θ	Looper angle
$\alpha_d^i(t)$	Looper angular acceleration
l	Looper arm length
M_t	Looper arm weight
$\dot{\theta}_d^i(t)$	Looper desired angular speed
J	Looper inertial momentum to the hydraulic actuator
LTCB	Looper torque calculation block
r	Looper roll diameter
M_a	Looper roller weight
$T_L(\theta)$	Looper weight torque
d	Pivot point distance from the pass line
υ	Poisson's ratio
S	Position of the roll
P_v	Process variable
K_p	Proportional gain
S_p	Setpoint
SMC	Sliding mode control
$S(t)$	Sliding surface
$K(x)$	Solution to Riccati equation
$\omega^i(t)$	Stand speed in rad/s
$Q(x)$	State weighting matrix in LQR
$A(x)$	State-dependent matrix
$C(x)$	State-dependent output matrix
$a(x)$	State-dependent vector
ρ	Steel density
$V(t)_i$	Strip entry speed to the *i*th stand
$v_i(t)$	Strip exit speed from the *i*th stand
H^i	Strip entry thickness
h^i	Strip exit thickness
$T_\sigma(\theta)$	Strip tension torque
$Q(x)$	State weighting matrix in LQR

Supplementary Information

The online version contains supplementary material available at https://doi.org/10.1186/s44147-022-00145-w.

Additional file 1. Fuzzy Control Rules [20, 21].

Additional file 2.

Additional file 3.

Additional file 4.

Additional file 5.

Additional file 6.

Additional file 7.

Additional file 8.

Additional file 9.

Additional file 10.

Additional file 11.

Additional file 12.

Additional file 13.

Additional file 14.

Additional file 15.

Additional file 16.

Additional file 17.

Additional file 18.

Additional file 19.

Additional file 20.

Additional file 21.

Additional file 22.

Additional file 23.

Additional file 24.

Acknowledgements
The authors would also like to thank ALLAH (Almighty) who strengthens us and supports us during this work.

Authors' contributions
AG developed the theoretical formalism, performed the analytic calculations, and performed the numerical simulations. Both AG and ME contributed to the final version of the manuscript. Both ME and HAF supervised the project. We confirm that the manuscript has been read and approved by all named authors and that there are no other persons who satisfied the criteria for authorship but are not listed. We further confirm that the order of authors listed in the manuscript has been approved by all of us.

Funding
This study had no funding from any resource.

Availability of data and materials
The datasets generated during and/or analysed during the current study are available from the corresponding author on reasonable request.

Declarations

Ethics approval and consent to participate
Not applicable.

Competing interests
The authors declare that they have no competing interests.

Received: 1 February 2022 Accepted: 13 September 2022
Published online: 27 October 2022

References

1. Li J, Zhong Z, Zhang J (2019) Inverse linear quadratic control for electric looper in hot strip finishing mill, 2019 Chinese Automation Congress (CAC). IEEE. pp. 5827–5832, https://doi.org/10.1109/CAC48633.2019.8996575
2. Li G, Sharifi FJ (2009) Fuzzy looperless tension control for hot. Fuzzy Sets Syst 160(4):521–536
3. Jung J-Y, Im Y-T (1999) Fuzzy control algorithm for the prediction of tension variations in hot rolling. J Mater Process Technol 96(1-3):163–172
4. Jiao XH, Shao LP, Peng Y (2011) Adaptive coordinated control for hot strip finishing mills. J Iron Steel Res Int 18(4):36–43
5. Imanari H et al (1997) Looper H-infinity control for hot-strip mills. IEEE Trans Ind Appl 33(3):790–796
6. Wang JC, Zhong ZZ (2011) Looper-tension H∞ control for hot strip finishing mills. J Shanghai JiaoTong Univ Sci 16(5):519–523
7. Wang H, Zhang K, Yu C (2018) Looper and tension control in hot rolling mills: an adaptive sliding mode approach, 2018 Chinese Control And Decision Conference (CCDC), pp. 3749–3754, https://doi.org/10.1109/CCDC.2018.8407774
8. Zhong Z, Wang J, Lu L (2010) Looper and tension control in hot strip finishing mills based on sliding mode and adaptive control. In: 2010 8th World Congress on Intelligent Control and Automation
9. Furlan, R., Cuzzola, F. A., & Parisini, T., Friction compensation in the interstand looper of hot strip mills: a sliding-mode control approach, Contrl Eng Pract, vol. 16, no. 2, pp. 214-224., 2008/2/1.
10. Sims RB (1954) The calculation of roll force and torque in hot rolling mils. Proc Inst Mechan Eng 168(1):191–200
11. Pittner J, Simaan MA (2010) A useful control model for tandem hot metal strip rolling. IEEE Trans Ind Appl 46(6):2251–2258
12. Lenard JG, Pietrzyk M, Cser L (1999) Mathematical and physical simulation of the properties of hot rolled products. Elsevier
13. Ford H, Ellis EF, Bland DR (1951) Cold rolling with strip tension. 1. A new approximate method of calculation and a comparison with other methods. J Iron Steel Inst 168(1):57–72
14. Roberts WL (1983) Hot rolling of steel. Marcel Dekker, New York
15. Hearns G, Bilkhu T (2012) Mass flow control for intercritical rolling in hot mills. GE Energy. Web. 2012, General Electric Company. GEA19936 (05/2012)

16. Nakagawa S, Miura H, Fukushima S, Amasaki J (1990) Gauge control system for a hot strip finishing mill. In: 29th IEEE Conference on Decision and Control
17. An BJ, Park SH, Kim BY, Yum TD, Kang DH, Lee MH (2001) Tension control system for hot strip mills. In: ISIE 2001, ISIE 2001. 2001 IEEE International Symposium on Industrial Electronics Proceedings (Cat. No.01TH8570), pp. 1452–1457 vol.3, https://doi.org/10.1109/ISIE.2001.931919
18. Hearns G, Grimble MJ (2000) Robust multivariable control for hot strip mills. ISIJ Int 40(10):995–1002
19. Li W, Slotine J-J (1991) Applied nonlinear control. Prentice hall, Englewood Cliffs
20. Prabha IS, Rao KD, Krishna DSR (2008) Fuzzy logic based intelligent controller design for an injection mould machine process control. Int J Adv Eng Sci Technol 10(1):98–103
21. Xin H, Huang T, Liu X, Tang X (2009) Temperature control system based on fuzzy self-adaptive PID controller. In: Third International Conference on Genetic and Evolutionary Computing

Publisher's Note